Hindawi
Advances in Materials Science and Engineering
Volume 2018, Article ID 9328317, 15 pages
https://doi.org/10.1155/2018/9328317

Research Article

Effect of Nd^{3+} Ion Concentration on the Corrosion Resistance of API X70 Steel in Chloride-Rich Environments

D. M. Martinez de la Escalera,[1] J. J. Ramos-Hernandez,[2] E. Porcayo-Palafox,[3] J. Porcayo-Calderon,[3] J. G. Gonzalez-Rodriguez,[3] and L. Martinez-Gomez[2,4]

[1]*Facultad de Ingeniería, Universidad Autónoma de Campeche, Campus V, Av. Ing. Humberto Lanz, 24085 Campeche, CAM, Mexico*
[2]*Instituto de Ciencias Físicas, Universidad Nacional Autónoma de México, Avenida Universidad s/n, 62210 Cuernavaca, MOR, Mexico*
[3]*CIICAp, Universidad Autónoma del Estado de Morelos, Avenida Universidad 1001, 62209 Cuernavaca, MOR, Mexico*
[4]*Corrosion y Protección (CyP), Buffon 46, 11590 México City, Mexico*

Correspondence should be addressed to J. Porcayo-Calderon; jporcayoc@gmail.com

Received 3 January 2018; Accepted 3 June 2018; Published 2 July 2018

Academic Editor: Yee-wen Yen

In this study, the effect of the addition of Nd^{3+} ions as a corrosion inhibitor of the API X70 steel in a medium rich in chlorides was evaluated. The performance of the Nd^{3+} ions was evaluated by means of electrochemical techniques such as potentiodynamic polarization curves, open circuit potential measurements, linear polarization resistance, and electrochemical impedance spectroscopy, as well as by means of scanning electron microscopy and EDS measurements. The results showed that Nd^{3+} ions reduce the corrosion rate of steel at concentrations as low as 0.001 M Nd^{3+}. At higher concentrations, the inhibition efficiency was only slightly affected although the concentration of chloride ions was increased by the addition of the inhibitor. The adsorption of the Nd^{3+} ions promotes the formation of a protective layer of oxides/hydroxides on the metal surface, thereby reducing the exchange rate of electrons. Nd^{3+} ions act as a mixed inhibitor with a strong predominant cathodic effect.

1. Introduction

In the last decades, there has been a great interest in the use of rare earth metals for the synthesis of compounds with inhibitory capacity of the corrosion of metals and alloys (Al, Fe, Mg, and Zn mainly) in aggressive environments. These compounds have been used as soluble elements in the electrolyte or as an additive of organic coatings. It has been recognized that rare earth salts are low-toxicity compounds whose average lethal dose (LD50) is similar to that of sodium chloride (NaCl) [1–3]; therefore, the interest in the use of rare earths has emerged as an alternative to replace those toxic and highly carcinogenic corrosion inhibitors that affect both people and the environment, and many of these dangerous inhibitors are based on chromates (CrO^{2-}_4), mercurate, nitrite, and alkynol [4]. Most of the studies have been reported based on the use of both Ce and La salts as corrosion inhibitors, in the form of either chlorides, nitrates, or other salts [2, 4–9]. Many of these studies have been carried out in chloride-rich solutions, and the excellent corrosion inhibiting capacity of rare earth salts has been attributed to the high reactivity of rare earths.

It is known that, in an electrochemical corrosion process, the cathodic reaction activates the O_2 reduction reaction causing an increase of the pH in the cathodic sites of the metallic surface [4]. It has been observed that this local increase in pH enhances the precipitation of rare earth ions, and this promotes the formation of a protective film of complex hydrated oxides on the cathode sites of the metal surface. The formed protective film reduces the rate of oxygen reduction and increases the cathodic polarization rate, thus causing a reduction in the corrosion potential as well as in the corrosion current density [2–4, 6, 7, 10].

In the literature, several studies can be found which indicate that various lanthanide base compounds possess excellent properties as corrosion inhibitors. In particular, the best anticorrosive properties have been detected mainly on light alloys, such as alloys based on aluminum, magnesium, and zinc [7–17]. However, some studies on iron-base alloys have also shown that rare earths and their compounds are capable of inhibiting the iron corrosion [4, 18–20]. Since iron is the main element of many structural alloys with applications in aqueous media rich in chlorides, then the constant search for alternatives to counteract the adverse effects of the corrosive environment is of interest.

Although the main technological applications of rare earths have been focused in the field of high technology electronics, from the point of view of their abundance, La, Ce, Pr, and Nd emerge as the main candidates to be used as corrosion inhibitors. In particular, the availability of Nd for the synthesis of corrosion inhibitors can be attractive if the new technologies for the recycling of rare earths are considered [21–24]. Therefore, in this study, the corrosion inhibitory capacity of neodymium chloride on API X70 steel in a 3.5% NaCl solution at room temperature is evaluated. However, because the neodymium chloride molecule is formed by one Nd atom, three Cl atoms, and six water molecules, in this study the inhibitory capacity is evaluated as a function of the amount of Nd^{3+} ions added instead of considering the entire molecule. The performance of the Nd^{3+} ions as a corrosion inhibitor is evaluated by means of electrochemical techniques such as potentiodynamic polarization curves, open circuit potential measurements, linear polarization resistance, and electrochemical impedance spectroscopy, and corroded specimens were analyzed by scanning electron microscopy and EDS measurements.

2. Experimental Procedure

2.1. Corrosion Inhibitor. The source of Nd^{3+} ions used in this study was neodymium chloride. This salt was obtained by dissolving neodymium oxide in a dilute solution of HCl until a clear solution was obtained. Subsequently, the solution was subjected to dryness at 60°C, and the resulting salt used in that condition was used for the corrosion tests.

$$Nd_2O_3 + 6HCl \longrightarrow 2NdCl_3 + 3H_2O \xrightarrow{\Delta} 2NdCl_3 \cdot 6H_2O \quad (1)$$

Because the neodymium chloride molecule is formed by approximately 40% of the Nd^{3+} cation, 30% of the Cl^- anion, and 30% of water (at.%), in this study and in order to avoid ambiguities, it was decided to evaluate the effect of the concentration of the rare earth cation as a corrosion inhibitor rather than the salt as a whole.

2.2. Electrochemical Evaluation. As a study material, an API X70 steel was used, from which specimens with dimensions 10*10*5 mm were obtained. A copper wire was welded by the spot-welding technique on one of the faces of the specimens, and in this condition, they were encapsulated in epoxy resin. The encapsulated specimens were roughened with abrasive paper from grade 120 to grade 1200 and subsequently polished with 0.5-micron diamond paste using ethanol as a lubricant. Subsequently, they were washed with distilled water and ethanol, dried, and used immediately in the corrosion tests.

As a corrosive medium, distilled water with 3.5% by weight of NaCl was used at room temperature under nonaerated conditions. The performance as a corrosion inhibitor of the neodymium chloride was determined, considering the concentration of Nd^{3+} ions added to the corrosive medium. In this sense, the concentrations of Nd^{3+} ions evaluated were 0.0001 M, 0.0005 M, 0.001 M, 0.005 M, and 0.01 M.

The electrochemical evaluation was performed in a three-electrode electrochemical cell using the encapsulated specimens as working electrodes, a saturated calomel electrode as the reference electrode, and a graphite bar with an area greater than that of the working electrode as a counter electrode. The electrochemical techniques used were potentiodynamic polarization curves (anodic and cathodic), open circuit potential measurements, linear polarization resistance measurements, and electrochemical impedance spectroscopy.

The anodic and cathodic branches of the polarization curves were obtained independently using a new working electrode in each case. The cathodic polarization curve was obtained by scanning cathodically the working electrode from +10 mV to −300 mV, and the anodic curves were obtained in a similar way but from −10 mV to 500 mV, in both cases with respect to its open circuit potential. In both cases, before starting the test, the electrochemical cell was allowed to stabilize for 24 hours before starting the scan at a speed of 0.1667 $mV \cdot s^{-1}$. The open circuit potential (OCP) measurements were carried out by recording the potential of the working electrode with respect to the reference electrode at intervals of one hour. For linear polarization resistance (RPL) measurements, the working electrode was polarized at ±10 mV with respect to its open circuit potential, the value of the polarization resistance was determined from the slope of the obtained E-I ratio, and measurements were made at one-hour intervals. The electrochemical impedance spectra (EIS) were obtained by applying an amplitude perturbation of 10 mV with respect to the open circuit potential of the working electrode in a frequency range from 100 kHz to 0.01 Hz. OCP, LPR, and EIS measurements were performed for 100 hours.

3. Results and Discussion

3.1. Potentiodynamic Polarization Curves. Figures 1 and 2 show the anodic and cathodic branches, respectively, of API X70 steel in 3.5% NaCl solution with the addition of Nd^{3+} ions at different concentrations. From both figures can be observed a cathodic direction shift of the corrosion potential, with respect to the blank, at concentrations greater than 0.0001 M Nd^{3+}, and this behavior is indicative of the existence of a cathodic inhibition process. In a similar way, a displacement is observed, with respect to the blank, of both anodic and cathodic branches towards lower current

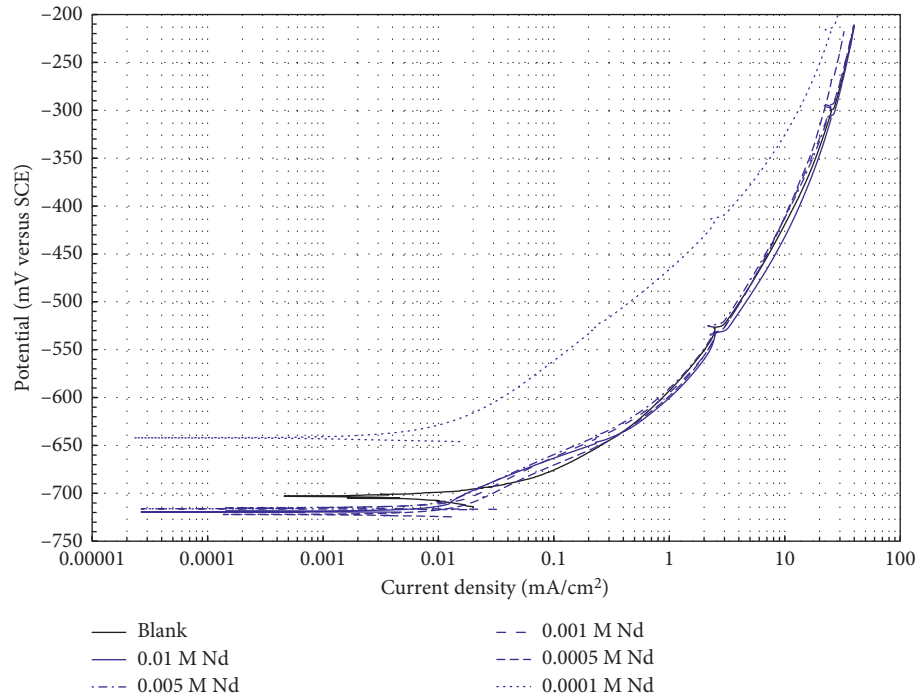

Figure 1: Anodic polarization curves for API X70 steel in 3.5% NaCl solution at different concentrations of Nd^{3+} ions (0.1667 mV·s^{-1}).

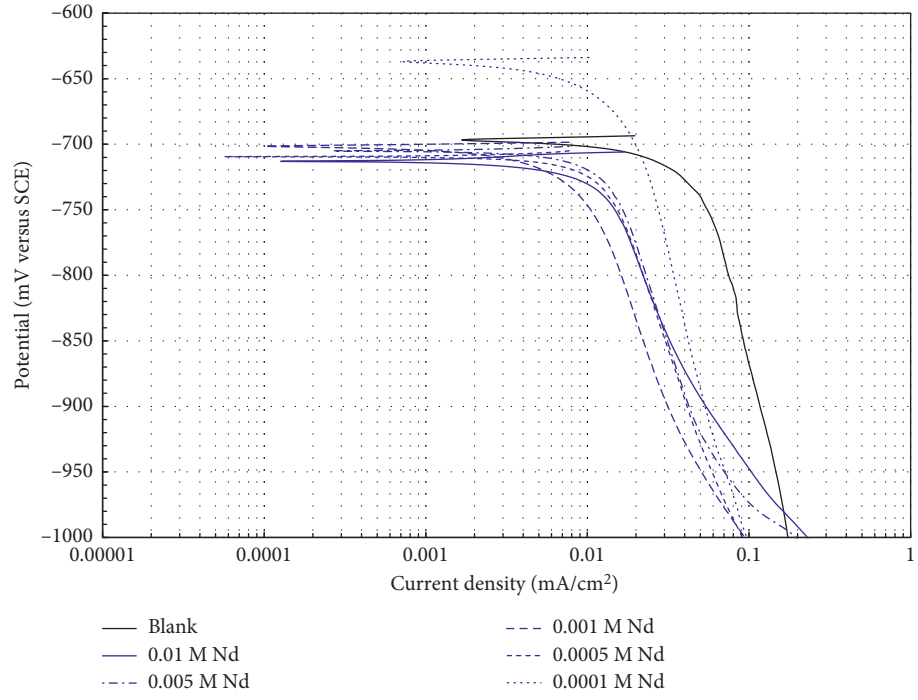

Figure 2: Cathodic polarization curves for API X70 steel in 3.5% NaCl solution at different concentrations of Nd^{3+} ions (0.1667 mV·s^{-1}).

densities. From the anodic branches, it is possible to observe a change in its slope to potentials slightly above the corrosion potential; this suggests that the presence of Nd^{3+} ions also affects the anodic reaction of the electrochemical corrosion process of the API X70 steel.

From the cathodic branch, it is possible to observe that the addition of Nd^{3+} ions caused a decrease in the cathodic current regardless of the concentration of added inhibitor. The greatest reduction in the cathodic current is observed at the concentration of 0.001 M Nd^{3+}. It has been suggested that the reduction observed in the cathodic current is due to the high concentration of OH^- ions in the cathode sites and to the high reactivity of the lanthanide ions, which by reacting form an insoluble oxide/hydroxide layer on the cathodic

Table 1: Electrochemical parameters of the polarization curves in the presence of Nd^{3+} ions.

(Nd^{3+}) M	Cathodic E_{corr} (mV)	Anodic E_{corr} (mV)	Ba (mV/Dec)	Bc (mV/Dec)	Anodic I_{corr} (mA/cm^2)	Cathodic I_{corr} (mA/cm^2)
0	−696	−703	72	517	0.0466173	0.047242
0.01	−713	−720	53	308	0.0107901	0.011432
0.005	−704	−716	56	380	0.0095416	0.0129336
0.001	−707	−714	57	346	0.0124705	0.0083153
0.0005	−713	−720	56	371	0.0120315	0.0126311
0.0001	−638	−642	92	645	0.0056876	0.0251889

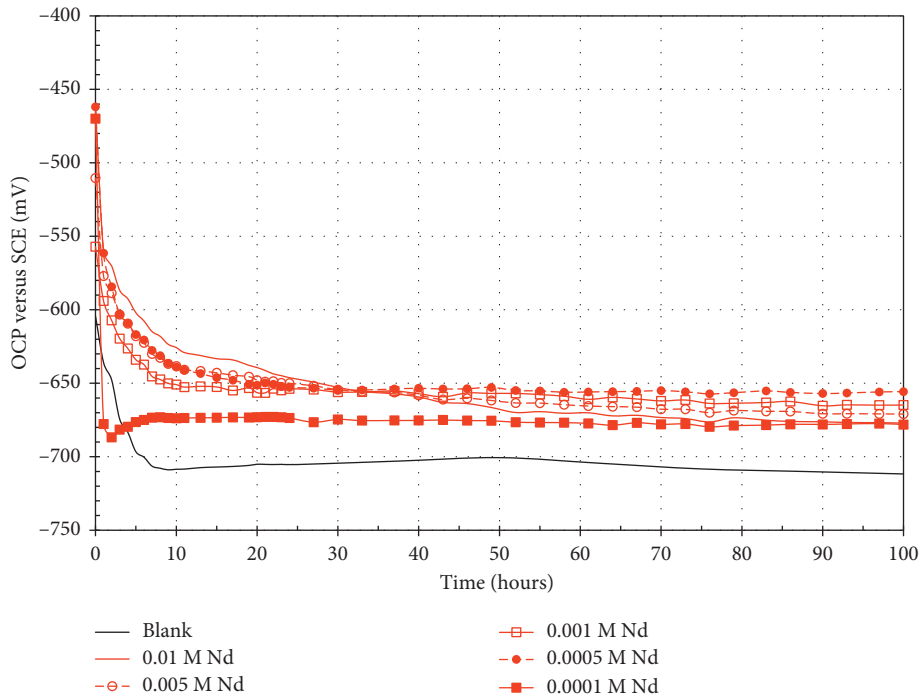

Figure 3: Variation in OCP values for API X70 steel in 3.5% NaCl solution at different concentrations of Nd^{3+} ions.

sites, reducing the cathodic reaction rate and the localized corrosion processes [2–4, 6, 7, 10].

Table 1 shows the electrochemical parameters extracted from the anodic and cathodic polarization curves. In general, it can be seen that there is a reduction in both anodic and cathodic slopes. This is due to the displacement towards lower current densities of both branches ($\Delta E/\Delta I$). The greatest reduction is observed in the cathodic slopes, which suggests a modification in the oxygen reduction reaction [7]. Only at the lowest concentration of Nd^{3+}, an increase in the cathodic slope was observed. On the other hand, although there was an increase in the Cl^- ion concentration due to the addition of the inhibitor, the anodic current density showed a decrease close to an order of magnitude. However, in the case of cathodic current density, the greatest decrease occurred at concentrations up to 0.001 M Nd^{3+}. Notwithstanding the beneficial effect of the rare earth chlorides on the corrosion inhibition process, their addition in high concentrations will cause a decrease in their inhibitory capacity due to the inherent increase of the chloride ions in the electrolyte [6].

It is known that the addition of an inhibitor can affect the overall corrosion process by affecting the anodic dissolution, the oxygen reduction, or both. In all three cases, a decrease in the corrosion current density is observed; however, a displacement of the corrosion potential towards more active potentials characterizes a cathodic inhibitor and in the opposite case to an anodic type. When an inhibitor affects both processes (corrosion current density and corrosion potential), it is considered as a mixed inhibitor, and its net effect in the polarization curves will be determined by the inhibition magnitude of the anodic and cathodic reactions [6]. The previous analysis shows that the addition of Nd^{3+} ions changed the corrosion process of the API X70 steel, affecting both the anodic and cathodic branches (different current densities); this suggests that both the local anodic dissolution and the cathodic reduction of oxygen are affected simultaneously [2, 4]. However, based on the negative displacement of the corrosion potential and the decrease of the cathodic current, it can be said that the Nd^{3+} ions act as mixed inhibitors with a predominant cathodic effect.

3.2. Open Circuit Potential Measurements. Figure 3 shows the variation in OCP values of API X70 steel in 3.5% NaCl solution as a function of time at different concentrations of

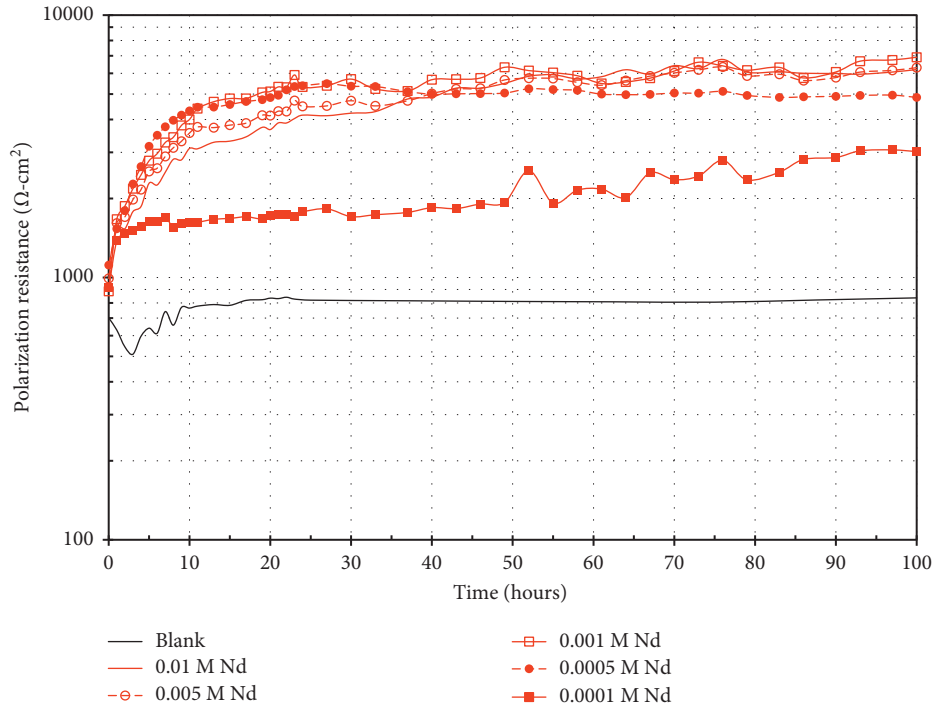

Figure 4: Variation in polarization resistance values for API X70 steel in 3.5% NaCl solution at different concentrations of Nd^{3+} ions.

Nd^{3+} ions. It is observed that, in the absence of Nd^{3+} ions, the steel showed an abrupt drop in its OCP values from approximately −600 mV to around −705 mV in the first 6 hours of immersion; afterwards, it showed a slight increase until 50 hours of immersion followed by a slight decrease in the rest of the test. It has been suggested that abrupt variations in OCP values at the beginning of the test may be a consequence of a reorganization of the surface layers due to the acceleration of the anodic process or a decrease in the activity of the cathodic process [4]. In the absence of Nd^{3+} ions, the most active OCP values were obtained. On the other hand, in the presence of Nd^{3+} ions, it is also possible to observe an abrupt drop in the OCP values at the beginning of the test, and subsequently after 50 hours of immersion, it is possible to observe a quasistationary state. It is known that the displacement of the OCP values to more active values besides being associated with an increase in the anodic reaction rate (metallic solution) can also correspond to the presence of an inhibition process of the cathodic reaction [2]. In the case of rare earth-based corrosion inhibitors in chloride-rich solutions, this displacement has been associated with the formation of a layer of rare earth products onto cathodic sites of the metal surface, blocking the reduction of dissolved oxygen [2, 23]. It is possible to observe that, regardless of the concentration of Nd^{3+} ions, the OCP values are within a band of 25 mV.

It has been suggested that a displacement in the OCP values greater than ±85 mV, with respect to the blank, is typical of anodic or cathodic inhibitors depending on the direction of displacement; otherwise, they are mixed inhibitors [24–26]. However, the results of this study show a variation in the OCP values lower than 85 mV; this reaffirms that the Nd^{3+} ions act as a mixed inhibitor with a strong predominant cathodic effect as previously established.

3.3. Linear Polarization Resistance Measurements. Figure 4 shows the variation in the polarization resistance values of API X70 steel as a function of time at different concentrations of Nd^{3+} ions. In the absence of inhibitor, oscillations in the polarization resistance values are observed in the first 10 hours of immersion, and a quasistationary state is subsequently observed. These variations are consistent with the observations established in the OCP measurements; that is, the initial behavior corresponds to a reorganization of the surface layer due to the acceleration of the anodic dissolution process [2, 4]. In the presence of Nd^{3+} ions in all cases, a significant increase in the polarization resistance values was observed in the first 10 hours of immersion and, subsequently, a less pronounced ascendant trend was observed with slight oscillations. These trends demonstrate the corrosion inhibitory capacity of Nd^{3+} ion. According to the graph at concentrations higher than 0.0005 M Nd^{3+}, similar polarization resistance values are observed.

Figure 5 shows the inhibition efficiency as a function of the concentration of Nd^{3+} ions. The calculation of the inhibition efficiency was according to the following expression:

$$E(\%) = \left(\frac{Rp_i - Rp_b}{Rp_i}\right) * 100, \quad (2)$$

where Rp_i corresponds to the polarization resistance in the presence of inhibitor and Rp_b corresponds to the polarization resistance in the absence of inhibitor. In each case, the

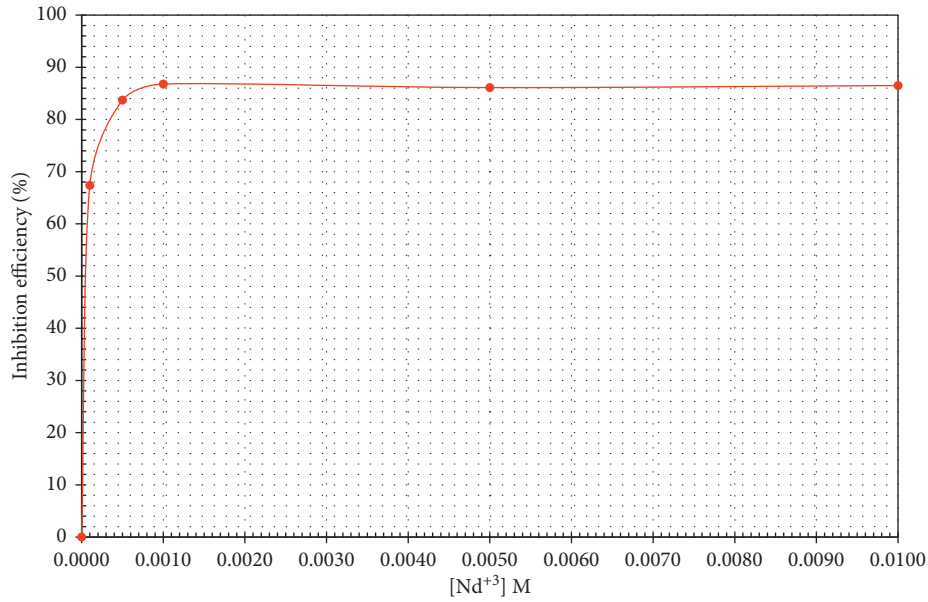

Figure 5: Effect of the concentration of Nd^{3+} ions on the corrosion inhibition efficiency of API X70 steel in 3.5% NaCl solution.

polarization resistance values used correspond to the average of the last 50 hours of the values reported in the previous figure. According to the graph, it is observed that the inhibition efficiency is close to 90% at concentrations higher than 0.0005 M Nd^{3+}. The highest inhibition efficiency was obtained with 0.001 M Nd^{3+}; at higher concentrations, the inhibition efficiency tends to decrease slightly, possibly due to the increase in the concentration of chloride ions.

3.4. Electrochemical Impedance Spectroscopy Measurements. Figure 6 shows the Nyquist and Bode diagrams for API X70 steel in 3.5% NaCl solution at different concentrations of Nd^{3+} ions after 100 hours of immersion. According to the Nyquist diagram, in the absence of inhibitor, the steel shows the presence of a depressed capacitive semicircle with a diameter less than 1000 Ω-cm^2. This is confirmed from the Bode diagram which shows the presence of a single time constant at frequencies around 10 Hz with a maximum phase angle close to 54°. From the evolution of the impedance module, $|Z|$, it is possible to define the high-frequency plateau (≥1000 Hz) which indicates the absence of some layer of corrosion products on its surface with viscous characteristics that affect the diffusion of species; however, the low-frequency plateau is not fully defined (≤1 Hz). On the other hand, in the presence of inhibitor, regardless of its concentration from the Nyquist diagram, the apparent presence of a single capacitive semicircle is also visible; however, the analysis of the Bode diagrams reveals the existence of three time constants. The fact that these are not visible in the Nyquist diagram is due to that the first two time constants emerge from the high-frequency region to the intermediate-frequency region, and the experimental points mostly visible correspond to the low-frequency region. According to the Bode diagram in its impedance module format, the first time constant is located in the high-frequency region around 10,000 Hz, the second time constant in the intermediate-frequency region from 10 to 200 Hz, and the third time constant at a frequency less than 1 Hz. Correspondingly, the three time constants are associated with a change in slope of the relation $\log f$ versus $\log |Z|$ at the indicated frequencies. The maximum values of impedance modulus are in agreement with the results of polarization resistance and inhibition efficiency that indicate that, with the addition of 0.001 M Nd^{3+}, the greater inhibition of the corrosion process is obtained.

Figure 7 shows the evolution of the impedance spectra as a function of time for API X70 steel with the addition of 0.001 M Nd^{3+}. Similar characteristics were observed at other concentrations. In general, from the Nyquist diagrams, the apparent presence of a single capacitive semicircle whose diameter increases as a function of time is observed. However, again from the Bode diagram in its phase angle format, the presence of three time constants is observed. It has been suggested that this is because in passive systems, the corrosion process is controlled by the reactions occurring at the interface with the electrolyte, and these are detected in the low-frequency region; therefore, the predominant signal in the Nyquist diagrams corresponds to response of these processes [4].

In the high-frequency region, the evolution (around 10,000 Hz) of the first time constant with a maximum phase angle of 28° is observed. In the intermediate-frequency region, the presence of the second time constant is observed around 5 Hz with a maximum phase angle of 60°, and in the low-frequency region (1 ≤ Hz), the third time constant is located with a maximum phase angle around 50°. In the impedance module format, $|Z|$, a slope change of the relation $\log f$ versus $\log |Z|$ associated with the presence of the three time constants is observed. It is also evident that the absence of the plateaus of both high- and low-frequency regions is due to the presence of a time constant in those regions. It is

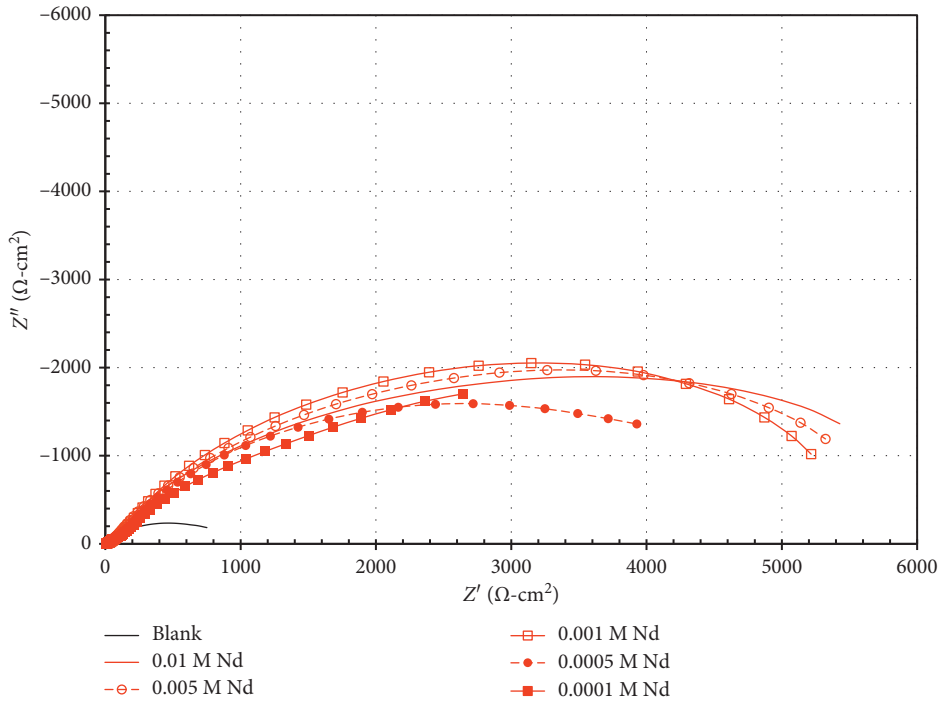

(a)

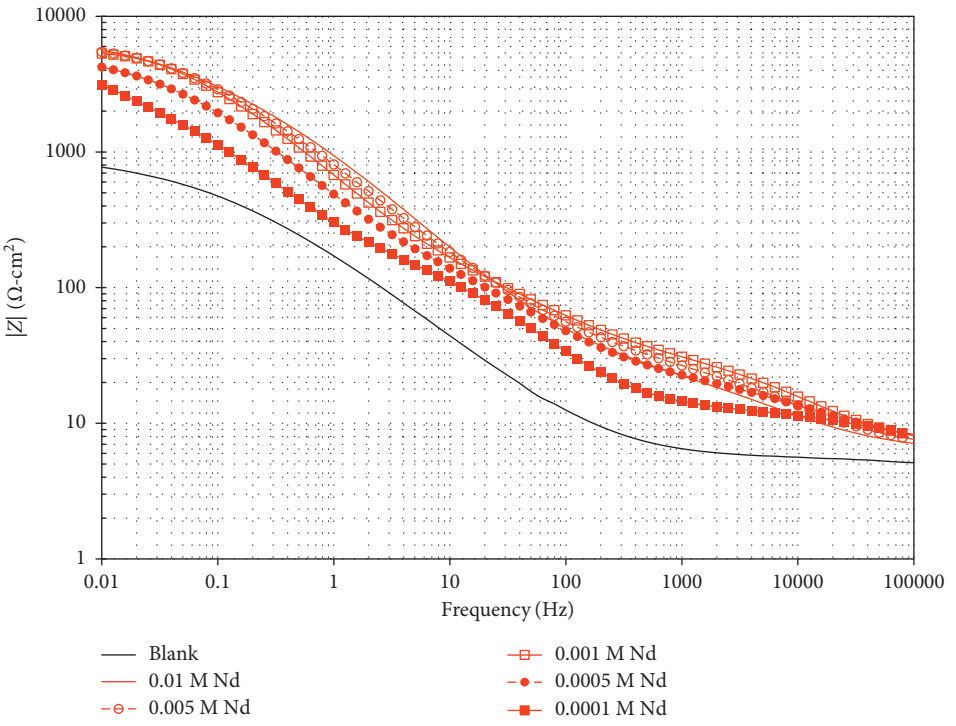

(b)

Figure 6: Continued.

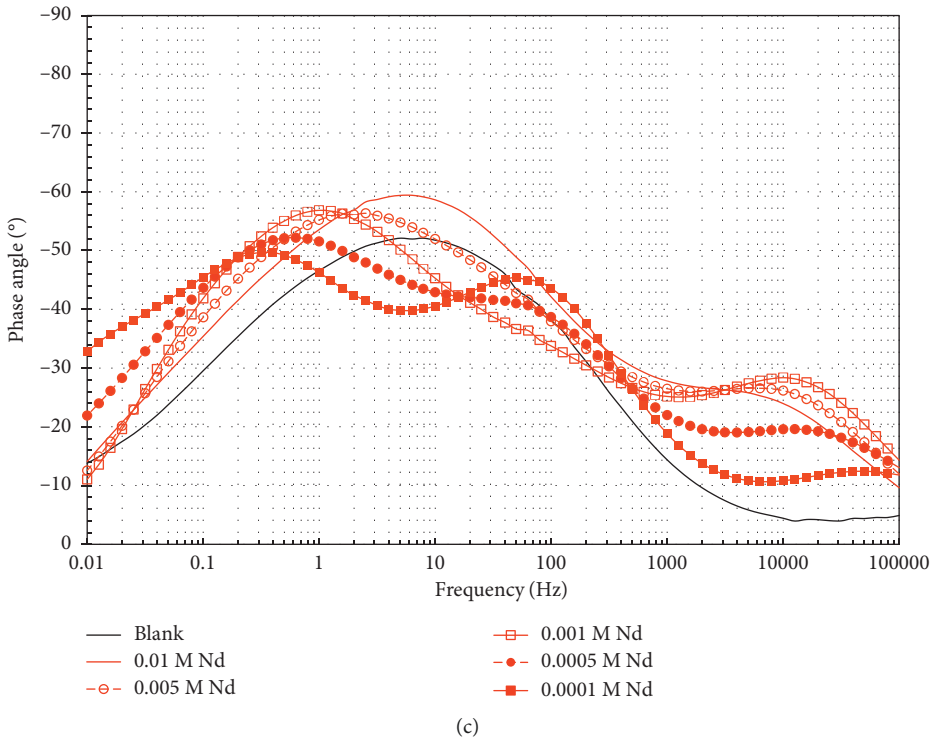

FIGURE 6: Nyquist and Bode diagrams for API X70 steel with and without the addition of Nd^{3+} ions after 100 hours of immersion in 3.5% NaCl solution.

possible that the absence of the high-frequency plateau is due to the presence of a surface layer on the working electrode, and the absence of the low-frequency plateau indicates that the maximum impedance module is greater than the last registered value, as well as the existence of a process of diffusion-adsorption of species on the surface of the working electrode.

It is evident that, in the presence of Nd^{3+} ions, there was a change in the mechanism of the corrosion process, and this can be attributed to the formation or deposition of an Nd oxide film on the metal surface. In general, the precipitation of the oxide layer is due to hydrolysis reactions of the metal cations with the OH^- ions produced at the cathodic sites. The increase in pH of the cathodic sites causes the precipitation of compounds of the type $Me(OH)_3$, which subsequently are transformed to more stable metal oxides (Me_2O_3). The mechanism of precipitation of both rare earth oxides and hydroxides has been cited in the literature previously [7, 27–30]. In general, the hydrolysis reaction of lanthanide cations (Ln) can occur according to the following reactions:

$$\begin{aligned} O_2 + 2H_2O + 4e^- &\longrightarrow 4OH^- \\ Ln^{3+} + OH^- &\longrightarrow Ln(OH)^{2+} \\ Ln^{3+} + 2OH^- &\longrightarrow Ln(OH)^{+} \\ Ln^{3+} + 3OH^- &\longrightarrow Ln(OH)_3\downarrow \end{aligned} \tag{3}$$

The hydrolysis reaction of the rare earth cations can be associated with the presence and evolution of the time constant observed in the high-frequency region. Because the rare earth hydroxides are only stable in alkaline environments, their stability will depend on the continuous production of OH^- ions, and this will allow their lateral growth by forming a three-dimensional film that inhibits the corrosion process. Because a decrease in pH will cause its dissolution, then its transformation to oxide can occur almost simultaneously with the formation of complex hydroxides.

$$2Ln(OH)_3 \longrightarrow Ln_2O_3 + 3H_2O \tag{4}$$

This reaction can be associated with the presence and evolution of the second time constant due to the formation of a protective film with hydrophobic characteristics. The hydrophobic nature of rare earth oxides has been associated with its unique electronic configuration characterized by the presence of nonaccessible metallic orbitals that reduce its affinity for water, and only the oxygen atoms attached directly to the rare earth are able to form hydrogen bonds with water molecules [31, 32]. Similar observations have been reported, indicating that, by increasing the atomic number of the lanthanides, their reactivity decreases due to the fact that the external electrons have more nuclear attraction [4].

The presence of the third time constant observed in the low-frequency region (the only visible capacitive semicircle in the Nyquist diagram) represents the capacitive response of the electrochemical double layer and the charge transfer resistance, and its evolution is due to the presence of the first two time constants.

Figure 8 shows the equivalent circuits used to fit the impedance spectra. To model the behavior of API X70 steel

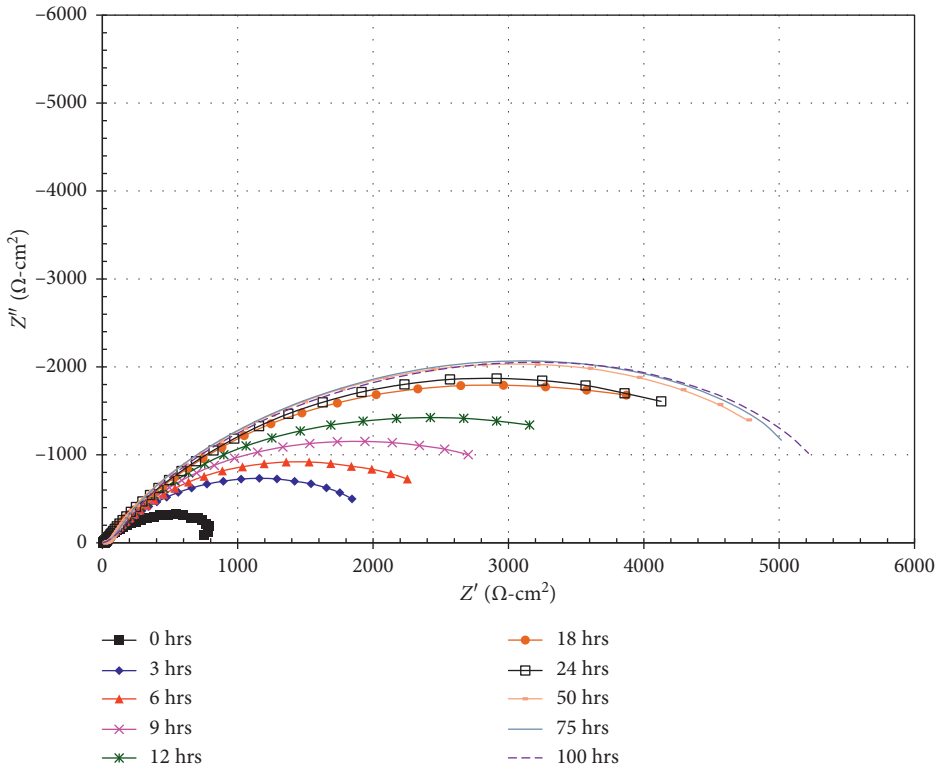

(a)

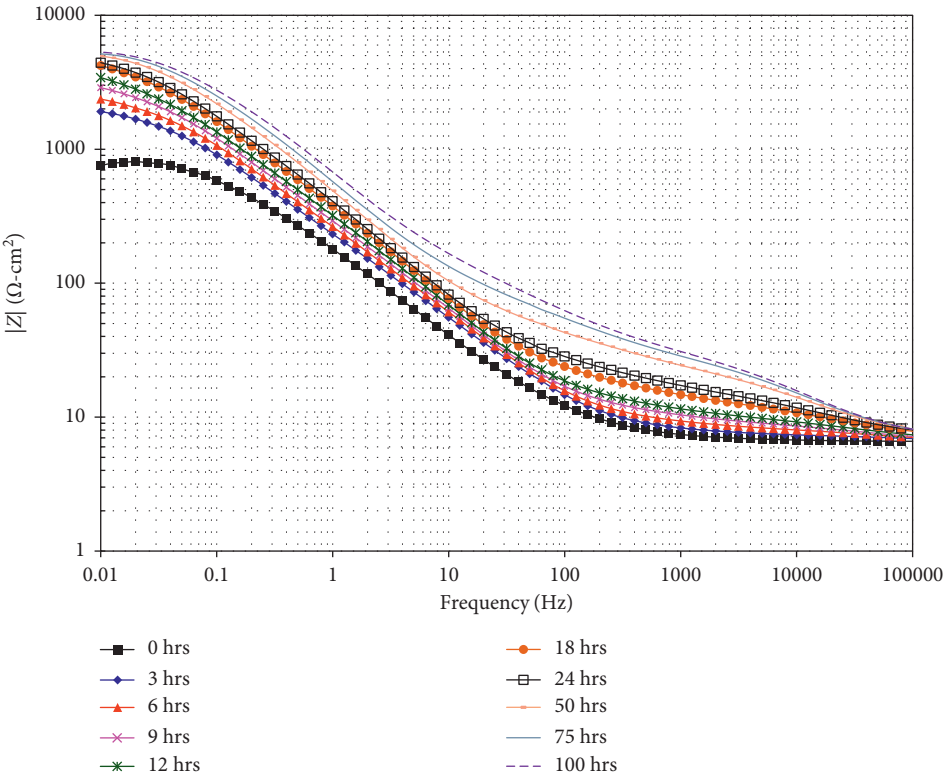

(b)

Figure 7: Continued.

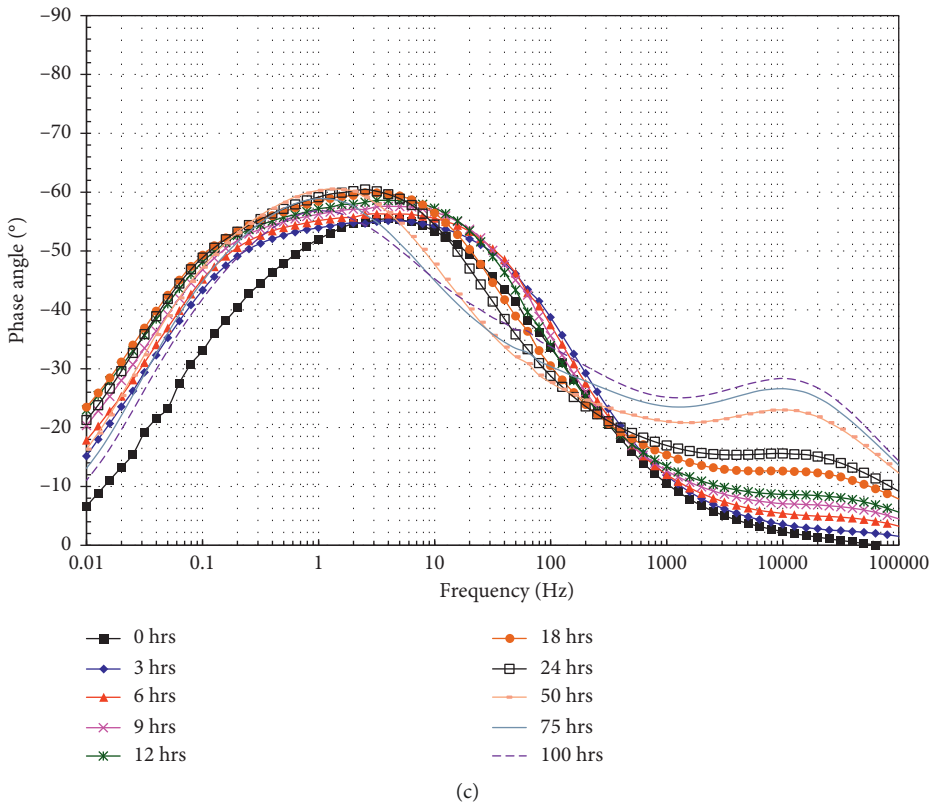

Figure 7: Evolution of the Nyquist and Bode diagrams for API X70 steel in 3.5% NaCl solution with the addition of 0.001 M Nd^{3+}.

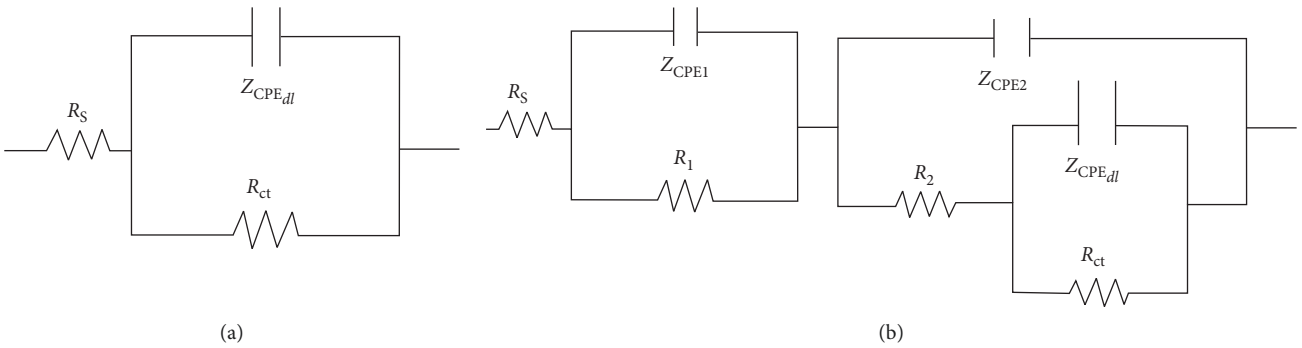

Figure 8: Proposed equivalent circuits for modeling the impedance spectra: (a) without the addition of Nd^{3+} ions and (b) with the addition of Nd^{3+} ions.

without the addition of Nd^{3+} ions, the equivalent circuit of Figure 8(a) was used; in this case, R_s is the electrolyte resistance, R_{ct} the charge transfer resistance, and $Z_{CPE_{dl}}$ the impedance of the double-layer capacitance. The constant phase element (CPE) was used in order to compensate the inhomogeneity due to the irregularities of the surface. The impedance of the CPE is defined as

$$Z_{CPE} = \frac{1}{Y_0}(i\omega)^{-n}, \quad (5)$$

where Y_0 is a proportional factor, i is the imaginary number, ω is the angular frequency ($\omega = 2\pi f$), f is the frequency, and n has the meaning of a phase shift.

On the other hand, with the addition of Nd^{3+} ions, the impedance spectra were modeled with the equivalent circuit of Figure 8(b). In this case, R_1 represents the resistance of the $Nd(OH)_3$ film adsorbed on the metal surface, R_2 represents the resistance of the Nd_2O_3 film precipitated on the metal surface, and Z_{CPE_1} and Z_{CPE_2} are the impedances of the constant phase elements of the $Nd(OH)_3$ film and of the Nd_2O_3 film, respectively.

The evolution of the fitting parameters of the impedance spectra after 100 hours of immersion (Figure 6) according the equivalent circuits of Figure 8 is shown in Table 2. From the R_{ct} data, the same tendency obtained in the other electrochemical measurements carried out can be observed;

Table 2: Evolution of electrochemical parameters of the EIS spectra after 100 hours of immersion in 3.5% NaCl solution.

Nd^{3+} ion concentration	R_1 (Ω-cm^2)	Y_{0_1} (μF·cm^{-2})	n_1	R_2 (Ω-cm^2)	Y_{0_2} (μF·cm^{-2})	n_2	R_{ct} (Ω-cm^2)	$Y_{0_{dl}}$ (μF·cm^{-2})	n_{ct}
0.0 M	—	—	—	—	—	—	848	$1.63E-3$	0.65
0.0001 M	15.92	$1.09E-3$	0.30	100.8	$1.31E-4$	0.87	4677	$1.06E-3$	0.63
0.0005 M	16.66	$1.49E-3$	0.59	141.0	$1.81E-4$	0.78	4971	$4.14E-4$	0.69
0.001 M	22.85	$3.98E-5$	0.69	161.4	$1.82E-4$	0.74	5950	$2.02E-4$	0.76
0.005 M	19.87	$4.80E-5$	0.69	41.0	$5.03E-5$	0.90	5886	$2.94E-4$	0.66
0.01 M	22.24	$2.03E-3$	0.60	7.9	$1.59E-4$	0.81	5770	$1.71E-4$	0.42

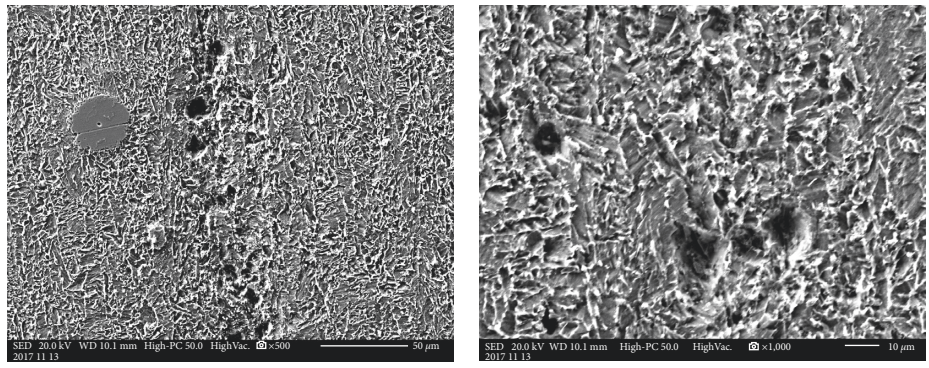

(a) (b)

Figure 9: Morphological aspect of API X70 steel after 100 hours of immersion in 3.5% NaCl solution.

that is, increasing the concentration of Nd^{3+} ions increases the corrosion resistance of the API X70 steel. The maximum charge transfer resistance is observed at a concentration of 0.001 M Nd^{3+}, and at higher concentrations, it decreases slightly. In addition, it can also be observed that, at this concentration, the resistance values of R_1 and R_2 are the highest, which also contribute to increase the corrosion resistance of the steel. This contribution can be observed by the values of n_{ct}, where the maximum value is also observed for the concentration of 0.001 M Nd^{3+}, which indicates a more capacitive surface.

3.5. Morphological Analysis of Corroded Surfaces. Figure 9 shows morphological aspects of the surface of the API X70 steel corroded for 100 hours in 3.5% NaCl solution in the absence of Nd^{3+} ions. The micrographs clearly show that the steel underwent a nonuniform corrosion process where pitting attack is evident. The absence of corrosion products indicates that the steel was not able to form a layer of protective corrosion products, suggesting the formation of soluble corrosion products.

The degradation of the steel occurred according to the basic reactions of iron oxidation and water reduction:

$$\begin{aligned} \mathrm{Fe} &\longleftrightarrow \mathrm{Fe}^{2+} + 2e^- \\ \mathrm{O_2} + 2\mathrm{H_2O} + 4e^- &\longleftrightarrow 4\mathrm{OH}^- \end{aligned} \tag{6}$$

In addition to the possible formation of nonprotective iron compounds such as hydroxides or oxyhydroxides, in addition to iron oxides,

$$\begin{aligned} \mathrm{Fe}^{2+} + 2\mathrm{OH}^- &\longleftrightarrow \mathrm{Fe(OH)_2} + \mathrm{H_2O} \\ 4\mathrm{Fe(OH)_2} + \mathrm{O_2} + 2\mathrm{H_2O} &\longleftrightarrow 4\mathrm{Fe(OH)_3} \\ 4\mathrm{Fe(OH)_2} + \mathrm{O_2} &\longleftrightarrow 2\mathrm{Fe_2O_3} + 4\mathrm{H_2O} \\ \mathrm{Fe(OH)_3} + \mathrm{O_2} &\longleftrightarrow \mathrm{FeOOH} + \mathrm{H_2O} \\ 4\mathrm{Fe(OH)_2} + \mathrm{O_2} &\longleftrightarrow 4\mathrm{FeOOH} + 2\mathrm{H_2O} \\ 2\mathrm{FeOOH} + \mathrm{H_2O} &\longleftrightarrow \mathrm{Fe_2O_3} + \mathrm{H_2O} \end{aligned} \tag{7}$$

Additionally, the presence of chloride ions promotes the formation of highly soluble iron chlorides and oxychlorides:

$$\begin{aligned} \mathrm{Fe}^{2+} + 2\mathrm{Cl}^- &\longleftrightarrow \mathrm{FeCl_2} \\ \mathrm{Fe}^{2+} + \mathrm{Cl}^- + \mathrm{H_2O} &\longleftrightarrow \mathrm{FeOCl} + \mathrm{H_2}\uparrow \end{aligned} \tag{8}$$

The attack experienced by the API X70 steel is correlated with the microstructure of the steel. It is known that depending on the manufacturing conditions and thermal treatments to which an X70 steel is subjected, its microstructure can be formed by the presence of different phases, the main being the polygonal ferrite, quasipolygonal ferrite, Widmanstätten ferrite, acicular ferrite, bainitic granular ferrite, bainite ferrite, martensite in addition to the presence of precipitates (Nb(CN), Fe_3C, MnS, and SiO_2) [33–35]. This combination of phases can favor a galvanic effect between them, causing the corrosion of the electrochemically less stable phase, generally the ferrite [36], in addition to a nonuniform distribution of the local anodic/cathodic ratio that favors localized corrosion [37]. The microstructure of the API X70 steel (Figure 10) was revealed by attacking the

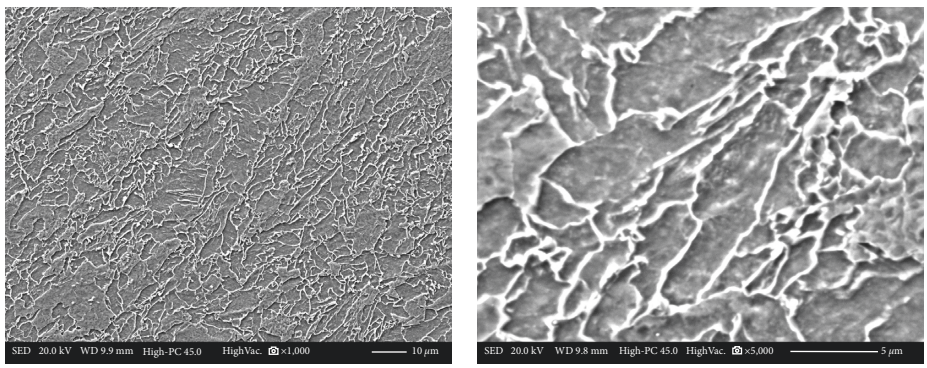

(a) (b)

Figure 10: Microstructure of the API X70 steel as received at different magnifications.

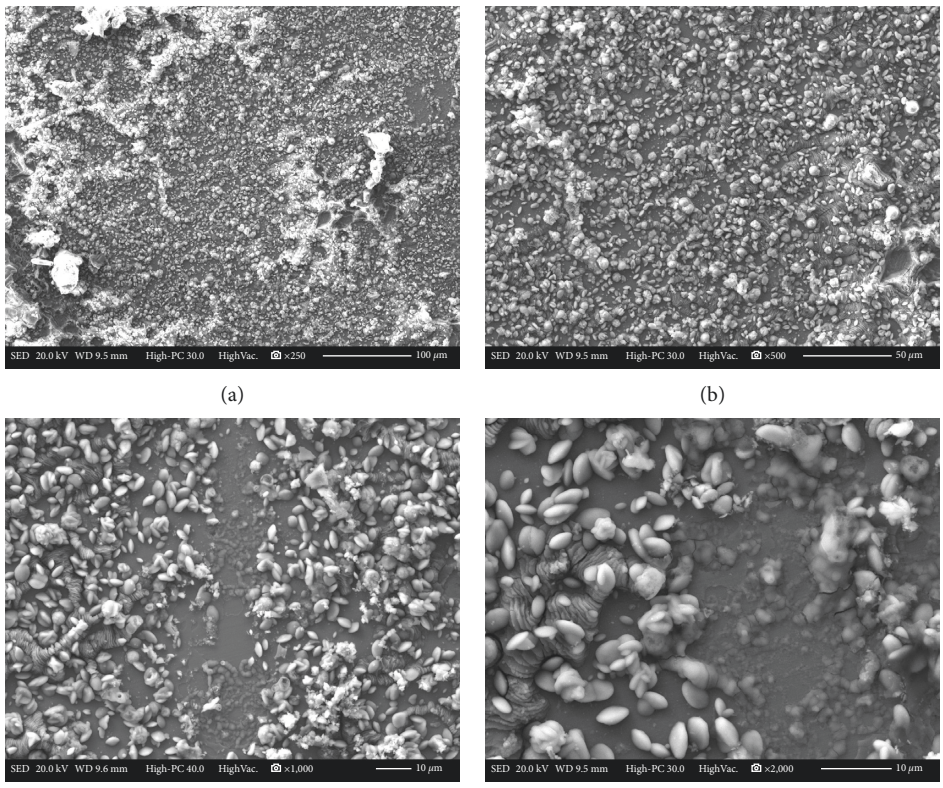

(a) (b)

(c) (d)

Figure 11: Surface appearance of the API X70 steel after 100 hours of immersion in 3.5% NaCl solution with the addition of 0.001 M Nd^{3+}.

steel with a 2% Nital solution (2 ml HNO_3 and 98 ml ethanol). According to the micrographs, it can be observed that the microstructure is composed of quasipolygonal ferrite grains, acicular ferrite, granular bainite, and perlite. Comparing the microstructure of the steel with the morphology of its surface after the corrosion process, it is possible to observe a great similarity between them. This similarity is in agreement with that mentioned above; the presence of multiple phases favors the appearance of galvanic pairs that reduce the resistance to corrosion of steel.

Figure 11 shows the morphological aspects of the surface of the API X70 steel corroded for 100 hours in 3.5% NaCl solution in the presence of 0.001 M Nd^{3+}. It is clearly observed that the surface appearance is completely different from that observed in the absence of inhibitor (Figure 9). The surface appearance shows the presence of a surface layer with protuberances, both morphologies possibly composed of Nd compounds.

A view at higher magnification (Figure 12) allows to define a thin layer adhered to the metal surface as well as

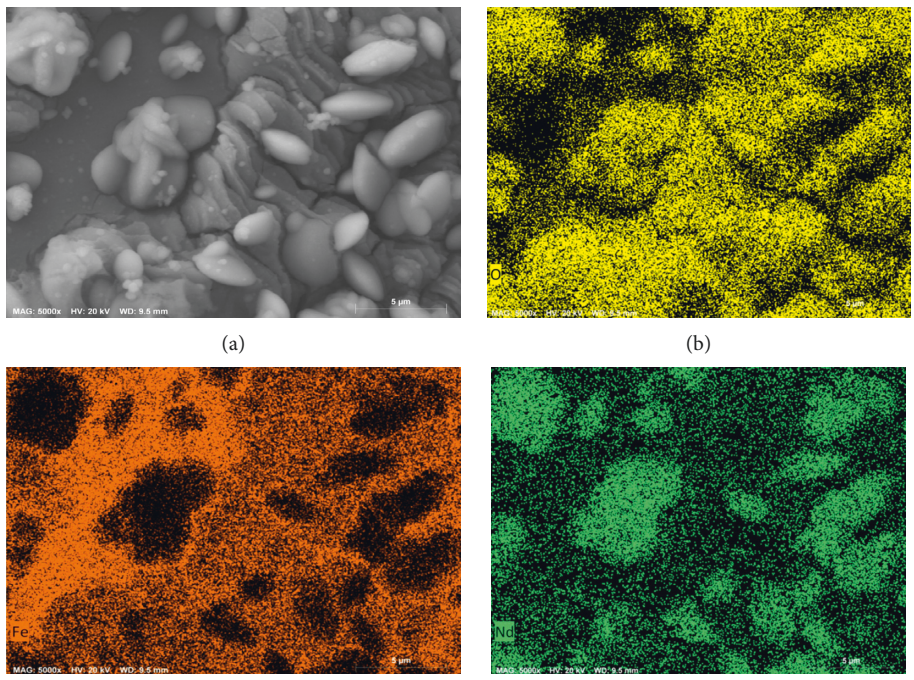

Figure 12: View to higher magnification to the corrosion product layer developed on the steel surface and mapping of elements.

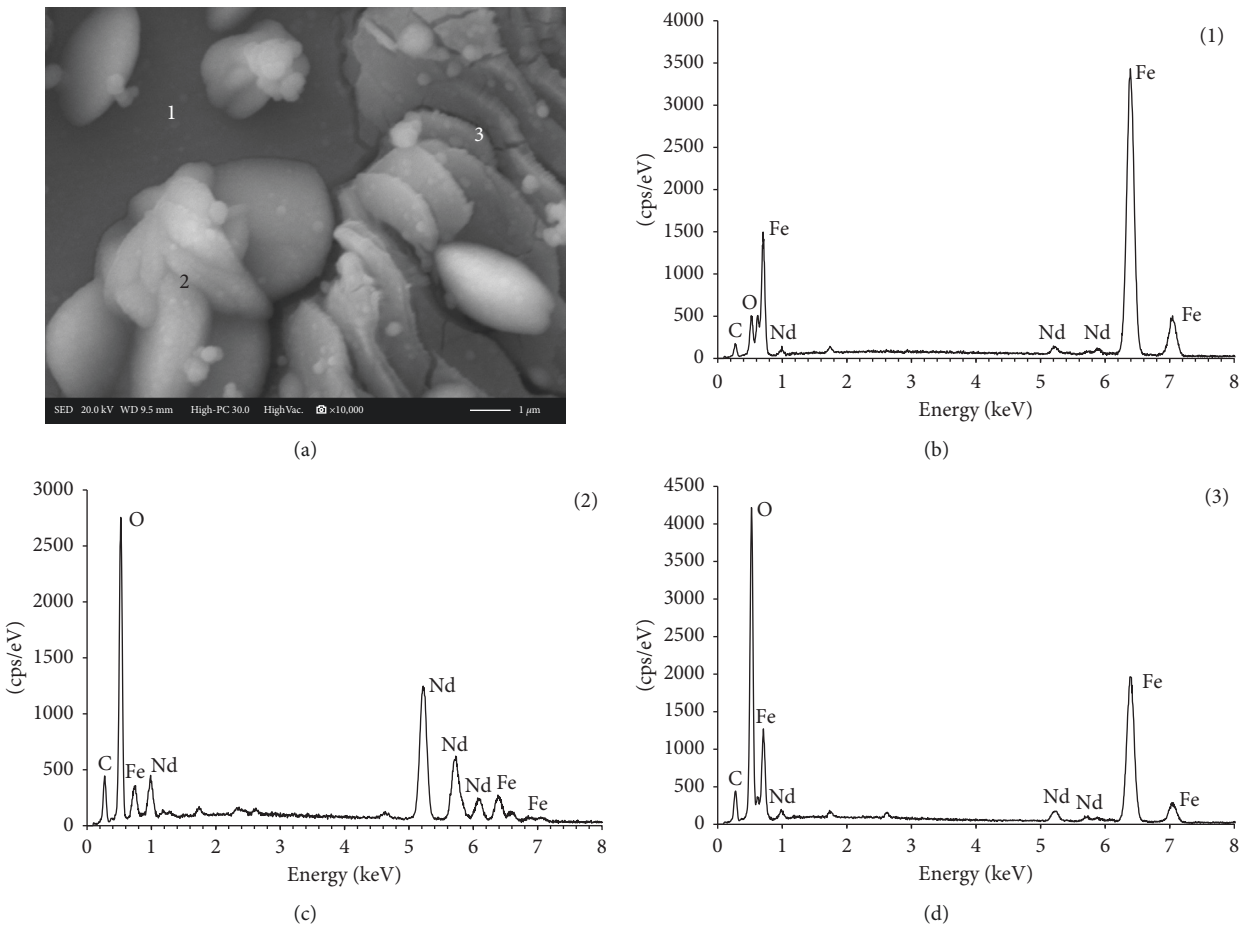

Figure 13: Elemental EDS analysis to the different morphologies observed on the API X70 steel surface.

the presence of multiple crystals in apparent cathodic sites on the surface of the steel. The mapping of elements shows the presence of Nd over the all surface, and its greater presence is detected in the crystals that protrude from the surface (Figure 12). A point analysis of the main morphologies identified (Figure 13) showed that the layer adhered to the surface (point 1) had an elemental composition of Fe = 92%, Nd = 3%, and O = 5% (% by weight), the crystals that protrude from the surface (point 2) had an elemental composition of Fe = 7%, Nd = 60%, and O = 33%, and the morphologies with the appearance of stacked layers (point 3) have an elemental composition of Fe = 54%, Nd = 7%, and O = 39%. According to the morphology of point 3, it is possible to deduce that the layer adhered to the metal surface had a thickness between approximately 200 and 400 nm.

It has been indicated that although the formation of a protective layer limits the exchange of electrons with the oxidizing species, the anodic and cathodic reactions are carried out through microdefects in the protective film [7]. Based on the observed evidence, it is possible to suggest that the Nd^{3+} ions protect the steel due to its adsorption on the metal surface forming a thin layer of oxyhydroxides. However, possibly the presence of imperfections causes the cracking and detachment of the protective layer forming the morphologies of stacked layers observed. In the case of small imperfections such as pores (cathode sites), the Nd^{3+} ions are able to precipitate and seal them, causing the formation of the small crystals identified as protuberances.

4. Conclusions

Measurements by means of different electrochemical techniques showed that Nd^{3+} ions are able to reduce the corrosion rate of API X70 steel in chloride-rich environments. Maximum protection is achieved in concentrations as low as 0.001 M Nd^{3+}. Regardless of the fact that, at higher concentrations, the concentration of Cl^- ions is increased and the protection efficiency is only slightly affected. Polarization curves and OCP measurements suggest that Nd^{3+} ions act as a mixed inhibitor with a strong predominant cathodic effect. According to the EIS measurements and morphological analysis, the presence of a protective layer composed of Nd oxides/hydroxides was observed. Although the thickness of the protective layer was 200–400 nm, its presence was able to reduce the exchange of electrons with the oxidizing species. However, the presence of microdefects on its surface caused the formation of morphologies such as stacked layers and protuberances due to the formation of active sites.

Data Availability

The data used to support the findings of this study are available from the corresponding author upon request.

Conflicts of Interest

The authors declare that there are no conflicts of interest regarding the publication of this paper.

Acknowledgments

Financial support from the Consejo Nacional de Ciencia y Tecnología (CONACYT, México) (Project 232611 "Laboratorio Nacional de Materias Primas, Metalurgia y Aleaciones Estratégicas Basadas en Tierras Raras Orientadas a Fortalecer la Sustentabilidad de los Sectores Energía, Transporte y Comunicaciones") is gratefully acknowledged. The authors are grateful for the comments and support provided by Dra M. Casales-Diaz.

References

[1] M. Bethencourt, F. J. Botana, J. J. Calvino, M. Marcos, and M. A. Rodriguez-Chacon, "Lanthanide compounds as environmentally-friendly corrosion inhibitors of aluminium alloys: a review," *Corrosion Science*, vol. 40, no. 11, pp. 1803–1819, 1998.

[2] D. Mohammedi, F. Ismail, R. Rehamnia, R. Bensalem, and O. Savadogo, "Corrosion behaviour of steel in the presence of rare earth salts: synergistic effect, corrosion engineering," *Science and Technology*, vol. 50, no. 8, pp. 633–638, 2015.

[3] M. A. Arenas, A. Conde, and J. J. de Damborenea, "Cerium: a suitable green corrosion inhibitor for Tinplate," *Corrosion Science*, vol. 44, no. 3, pp. 511–520, 2002.

[4] Z. Yanhua, Z. Jia, Y. Yongsheng, and Z. Xianguang, "Research on anti-corrosion property of rare earth inhibitor for X70 steel," *Journal of Rare Earths*, vol. 31, no. 7, pp. 734–740, 2013.

[5] H. Allachi, F. Chaouket, and K. Draoui, "Corrosion inhibition of AA6060 aluminium alloy by lanthanide salts in chloride solution," *Journal of Alloys and Compounds*, vol. 475, no. 1-2, pp. 300–303, 2009.

[6] S. Bernal, F. J. Botana, J. J. Calvino, M. Marcos, J. A. Perez-Omil, and H. Vidal, "Lanthanide salts as alternative corrosion inhibitors," *Journal of Alloys and Compounds*, vol. 225, no. 1-2, pp. 638–641, 1995.

[7] B. Davó and J. J. De Damborenea, "Use of rare earth salts as electrochemical corrosion inhibitors for an Al–Li–Cu (8090) alloy in 3.56% NaCl," *Electrochimica Acta*, vol. 49, no. 27, pp. 4957–4965, 2004.

[8] D. Ho, N. Brack, J. Scully, T. Markley, M. Forsyth, and B. Hinton, "Cerium dibutylphosphate as a corrosion inhibitor for AA2024-T3 aluminum alloys," *Journal of The Electrochemical Society*, vol. 153, no. 9, pp. B392–B401, 2006.

[9] H. Allachi, F. Chaouket, and K. Draoui, "Protection against corrosion in marine environments of AA6060 aluminium alloy by cerium chlorides," *Journal of Alloys and Compounds*, vol. 491, no. 1-2, pp. 223–229, 2010.

[10] X.-B. Chen, T. Cain, J. R. Scully, and N. Birbilis, "Technical note: experimental survey of corrosion potentials for rare earth metals Ce, Er, Gd, La, and Nd as a function of pH and chloride concentration," *Corrosion*, vol. 70, no. 4, pp. 323–328, 2013.

[11] D. R. Arnott, B. R. W. Hinton, and N. E. Ryan, "Cationic-film-forming inhibitors for the protection of the AA 7075 aluminum alloy against corrosion in aqueous chloride solution," *Corrosion*, vol. 45, no. 1, pp. 12–18, 1989.

[12] Y. Xingwen, C. Chunan, Y. Zhiming, Z. Derui, and Y. Zhongda, "Study of double layer rare earth metal conversion coating on aluminum alloy LY12," *Corrosion Science*, vol. 43, no. 7, pp. 1283–1294, 2001.

[13] M. Forsyth, T. Markley, D. Ho et al., "Inhibition of corrosion on AA2024-T3 by new environmentally friendly rare earth

organophosphate compounds," *Corrosion*, vol. 64, no. 3, pp. 191–197, 2008.

[14] D. Zhao, J. Sun, L. Zhang, Y. Tan, and J. Li, "Corrosion behavior of rare earth cerium based conversion coating on aluminum alloy," *Journal of Rare Earths*, vol. 28, pp. 371–374, 2010.

[15] Y. Shengxue, L. Qiaoyan, H. Jing, Z. Zhanwei, and Z. Qianyun, "Preparation and performance of rare earths chemical conversion film on magnesium alloy," *Journal of Rare Earths*, vol. 24, no. 1, pp. 397–400, 2006.

[16] L. Li, J. Lei, S. Yu, Y. Tian, Q. Jiang, and F. Pan, "Formation and characterization of cerium conversion coatings on magnesium alloy," *Journal of Rare Earths*, vol. 26, no. 3, pp. 383–387, 2008.

[17] S.-X. Yu, J.-Y. Cao, L. Chen, J. Han, and R.-J. Zhang, "Corrosion resistance, composition and structure of RE chemical conversion coating on magnesium alloy," *Transactions of Nonferrous Metals Society of China*, vol. 18, pp. s349–s353, 2008.

[18] F. Blin, S. G. Leary, G. B. Deacon, P. C. Junk, and M. Forsyth, "The nature of the surface film on steel treated with cerium and lanthanum cinnamate based corrosion inhibitors," *Corrosion Science*, vol. 48, no. 2, pp. 404–419, 2006.

[19] X. Li, S. Deng, H. Fu, G. Mu, and N. Zhao, "Synergism between rare earth cerium (IV) ion and vanillin on the corrosion of steel in H_2SO_4 solution: weight loss, electrochemical, UV–vis, FTIR, XPS, and AFM approaches," *Applied Surface Science*, vol. 254, no. 17, pp. 5574–5586, 2008.

[20] X. Cui, Y. Yang, E. Liu, G. Jin, J. Zhong, and Q. Li, "Corrosion behaviors in physiological solution of cerium conversion coatings on AZ31 magnesium alloy," *Applied Surface Science*, vol. 257, no. 23, pp. 9703–9709, 2011.

[21] G. G. Zaimes, B. J. Hubler, S. Wang, and V. Khanna, "Environmental life cycle perspective on rare earth oxide production," *ACS Sustainable Chemistry & Engineering*, vol. 3, no. 2, pp. 237–244, 2015.

[22] Z. Sun, Y. Xiao, H. Agterhuis, J. Sietsma, and Y. Yang, "Recycling of metals from urban mines–a strategic evaluation," *Journal of Cleaner Production*, vol. 112, pp. 2977–2987, 2016.

[23] M. A. Arenas and J. J. De Damborenea, "Growth mechanisms of cerium layers on galvanised steel," *Electrochimica Acta*, vol. 48, no. 24, pp. 3693–3698, 2003.

[24] O. L. Riggs Jr., Corrosion Inhibition, C. C. Nathan, Ed., National Association of Corrosion Engineers, Houston, TX, USA, 2nd edition, 1973.

[25] M. A. Amin, M. A. Ahmed, H. A. Arida et al., "Monitoring corrosion and corrosion control of iron in HCl by non-ionic surfactants of the TRITON-X series–Part III. Immersion time effects and theoretical studies," *Corrosion Science*, vol. 53, no. 5, pp. 1895–1909, 2011.

[26] M. S. Al-Otaibi, A. M. Al-Mayouf, M. Khan, A. A. Mousa, S. A. Al-Mazroa, and H. Z. Alkhathlan, "Corrosion inhibitory action of some plant extracts on the corrosion of mild steel in acidic media," *Arabian Journal of Chemistry*, vol. 7, no. 3, pp. 340–346, 2014.

[27] K. A. Yasakau, M. L. Zheludkevich, S. V. Lamaka, and M. G. S. Ferreira, "Mechanism of corrosion inhibition of AA2024 by rare-earth compounds," *Journal of Physical Chemistry B*, vol. 110, no. 11, pp. 5515–5528, 2006.

[28] E. A. Matter, S. Kozhukharov, M. Machkova, and V. Kozhukharov, "Comparison between the inhibition efficiencies of Ce(III) and Ce(IV) ammonium nitrates against corrosion of AA2024 aluminum alloy in solutions of low chloride concentration," *Corrosion Science*, vol. 62, pp. 22–33, 2012.

[29] T. Hu, H. Shi, T. Wei, F. Liu, and S. Fan, "En-Hou Han, cerium tartrate as a corrosion inhibitor for AA 2024-T3," *Corrosion Science*, vol. 95, pp. 152–161, 2015.

[30] L. J. Zhang, Z. Zhang, J. Q. Zhang, and C. N. Cao, "The study of the $La(NO_3)_3$ inhibition on X70 pipeline steel in 3.0(wt.%) NaCl solution," *Materials and Corrosion*, vol. 56, no. 9, pp. 630–635, 2005.

[31] G. Carchini, M. García-Melchor, Z. Łodziana, and N. Lopez, "Understanding and tuning the intrinsic hydrophobicity of rare-earth oxides: A DFT+U study," *ACS Applied Materials & Interfaces*, vol. 8, no. 1, pp. 152–160, 2016.

[32] R. Lundy, C. Byrne, J. Bogan et al., "Exploring the role of adsorption and surface state on the hydrophobicity of rare earth oxides," *ACS Applied Materials & Interfaces*, vol. 9, no. 15, pp. 13751–13760, 2017.

[33] B. Hwang, Y. M. Kim, S. Lee, N. J. Kim, and S. S. Ahn, "Correlation of microstructure and fracture properties of API X70 pipeline steels," *Metallurgical and Materials Transactions A*, vol. 36, no. 3, pp. 725–739, 2005.

[34] Y.-B. Guo, C. Li, Y.-C. Liu et al., "Effect of microstructure variation on the corrosion behavior of high-strength low-alloy steel in 3.5wt% NaCl solution," *International Journal of Minerals, Metallurgy, and Materials*, vol. 22, no. 6, pp. 604–612, 2015.

[35] T. V. Shibaeva, V. K. Laurinavichyute, G. A. Tsirlina, A. M. Arsenkin, and K. V. Grigorovich, "The effect of microstructure and non-metallic inclusions on corrosion behavior of low carbon steel in chloride containing solutions,," *Corrosion Science*, vol. 80, pp. 299–308, 2014.

[36] C. W. Du, X. G. Li, P. Liang, Z. Y. Liu, G. F. Jia, and Y. F. Cheng, "Effects of microstructure on corrosion of X70 pipe steel in an alkaline soil," *Journal of Materials Engineering and Performance*, vol. 18, no. 2, pp. 216–220, 2009.

[37] M. Alizadeh and S. Bordbar, "The influence of microstructure on the protective properties of the corrosion product layer generated on the welded API X70 steel in chloride solution,," *Corrosion Science*, vol. 70, pp. 170–179, 2013.